Inorganic Chemistry

Article

pubs.acs.org/IC

Novel Chemical Synthesis and Characterization of $CeTi_2O_6$ Brannerite

Linggen Kong,* Daniel J. Gregg, Inna Karatchevtseva, Zhaoming Zhang, Mark G. Blackford, Simon C. Middleburgh, Gregory R. Lumpkin, and Gerry Triani

Institute of Materials Engineering, Australian Nuclear Science and Technology Organisation, Locked Bag 2001, Kirrawee DC, NSW 2232, Australia

Supporting Information

ABSTRACT: Cerium titanate $CeTi_2O_6$ was prepared by a new soft chemistry route in aqueous solution. A suite of characterization techniques, including X-ray diffraction, thermal analysis, vibrational spectroscopy, and scanning and transmission electron spectroscopy, were employed to investigate the brannerite structure formation and its bulk properties. The synthesized powder formed the brannerite crystal structure upon calcination at temperatures as low as 800 °C. Samples sintered at 1350 °C possess a high level of crystallinity. X-ray absorption near-edge structure results indicate the presence of six-coordinated Ce^{4+} in the brannerite samples.

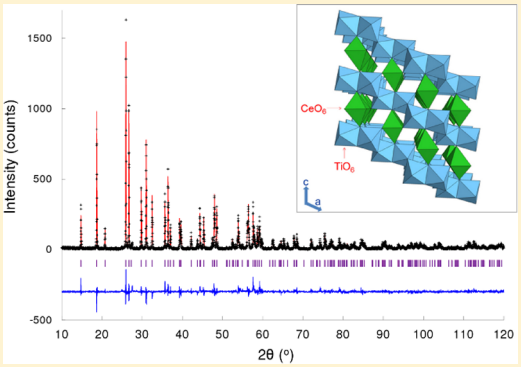

1. INTRODUCTION

Cerium titanates, including those with the brannerite structure, have many important applications as photocatalytic and ferroelectric materials, antireflective coatings, electrochromic layers, and self-cleaning glasses.[1−4] In addition, titanate ceramics with compositions MTi_2O_6 (M = U, Th, Ce) are important actinide host matrixes for the immobilization of actinide-bearing radioactive waste from nuclear power plants and weapons programs, with subsequent storage of the waste form in a geological repository.[5] Even though brannerite is a minor phase in synroc-type pyrochlore-rich waste forms,[5] the pure end-member composition (UTi_2O_6) contains 62.8 wt % UO_2. Therefore, it can account for a significant fraction of the total amount of actinides in the bulk solid.[5] Cerium is often considered an actinide "simulator" for uranium and plutonium because of the similar ionic radius, coordination environment, and oxidation states that can be attained.[5−13]

The MTi_2O_6 brannerite crystal structure belongs to the monoclinic crystal system, with space group *C*2/*m* and comprises planes of anatase-like corner and edge-sharing TiO_6 octahedra that form layers in the *ab* plane. These layers are linked along the *c* axis by MO_6 octahedra.[14]

The most common method for the preparation of cerium brannerite is by the mixed-oxide route.[6−13] Under this process, conventional solid-state reactions take place at 1350 °C with a required time of over 96 h and repeated grinding of the component oxides to allow interdiffusion of the cations.[6,7,11] Some common problems in processing solid solutions include uneven grain growth and segregation of dopant oxides, thus producing nonuniform microstructures. As a result, calcined powders are likely to show agglomeration and compositional heterogeneity. Physical properties such as electrical and optical characteristics are strongly influenced by the particulate morphology, compositional homogeneity, and the final microstructure.

In order to improve the material properties, several chemical synthetic methods for the titanate brannerites have been developed. The principal benefit of solution synthesis techniques in contrast to conventional solid-state reactions is the high chemical homogeneity achieved on the molecular scale in solution. These wet chemical routes include sol−gel synthesis,[1−4] alkoxide/nitrate route,[15−18] and the Pechini polymerization complex method.[19] Nevertheless, they each have specific drawbacks, for instance, the alkoxide-based sol−gel technologies[1−4,15−18] usually utilize moisture-sensitive alkoxides and need to be processed under an inert atmosphere. Otherwise, heterogeneous reactions occur due to extremely fast hydrolysis and polycondensation commonly found with titanium alkoxides. Although the sol−gel route ensures good mixing of the reactant species at the molecular level, the reaction between the dopant and the host species still proceeds via solid-state reaction.[20] Better chemical homogeneity may be achieved using the polymerizable complex method;[19] however, this process requires a large amount of stabilization agent (citric acid) and polymerization agent (poly(ethylene glycol)).

In order to produce high purity and homogeneous materials, alternate chemical strategies can be employed. In this study, a chemical synthesis pathway using non-moisture-sensitive precursors is investigated to produce $CeTi_2O_6$ brannerite. We report a very simple method for the preparation of cerium brannerite powder in an aqueous medium by employing

Received: March 11, 2014
Published: June 13, 2014

   dx.doi.org/10.1021/ic500563j | *Inorg. Chem.* 2014, 53, 6761−6768

Table 1. Summary of the XRD and SEM Results and Porosity Analysis of Pelletized Powder

sample	phases present	bulk density ($g \cdot cm^{-3}$)	apparent porosity (%)	% of theoretical density[a]
$CeTi_{2.0}$	$CeTi_2O_6$ + trace CeO_2	4.12	15.8	82.8
$CeTi_{2.1}$	$CeTi_2O_6$ + trace TiO_2	4.12	15.5	82.9
$CeTi_{2.2}$	$CeTi_2O_6$ + trace TiO_2	4.26	12.6	85.8

[a]The theoretical density of 4.97 $g \cdot cm^{-3}$ was determined based on the unit cell volume derived from X-ray diffraction data (see Table 2) and molecular weight based on full occupancy (i.e., $CeTi_2O_6$).

titanium(IV) bis(ammonium lactato)dihydroxide liquid (Tyzor LA) as a starting material, which is readily available in bulk quantities and has a long shelf life. The complex compound formation between Ce^{3+} [cerium(III) nitrate] and Tyzor LA occurs on a molecular level, which ensures homogeneity of the final product. Unlike traditional sol–gel processing, there is no organic solvent involved during synthesis and no milling step is required involving nonpolar solvents (e.g., cyclohexane) that prevent metal ions from dissolving. To the best of our knowledge, this is the first report of the preparation of cerium brannerite powder using Tyzor LA. This study also details the structural evolution of the synthesized powder following heat treatment and investigates the densification of the pelletized synthetic powder.

2. EXPERIMENTAL SECTION

Materials and Method. Tyzor LA, titanium(IV) bis(ammonium lactato)dihydroxide solution (50 wt % in water), and cerium(III) nitrate hexahydrate (99.9%+) were purchased from Aldrich and used as received. The titanium content in Tyzor LA was determined by gravimetric analysis. Milli-Q grade water was used in all experimental procedures. For a typical synthesis, the calculated mole ratios of Tyzor LA solution and cerium(III) nitrate hexahydrate salt were dissolved in water to form a solution upon stirring. The solution was dried overnight at 80 °C in an oven and subsequently sintered in a furnace in air between 800 and 1400 °C.

As a result of previously reported Ce deficiency in Ce brannerite,[7] powders with different Ti and Ce molar ratios were investigated. Samples $CeTi_{2.0}$, $CeTi_{2.1}$, and $CeTi_{2.2}$ were synthesized using Ti and Ce precursors in the molar ratios of 2.0, 2.1, and 2.2, respectively. XRD and SEM results indicate that all compositions contain trace amounts of either CeO_2 or TiO_2 rutile impurities. Since the formation of CeO_2 is not desirable for nuclear waste form applications and a molar ratio of Ce:Ti = 1:2.1 leads to the least amount of TiO_2 rutile with the brannerite main phase, the $CeTi_{2.1}$ composition is selected as the focus of our investigations.

Characterization. Differential scanning calorimetry (DSC) was performed between room temperature and 1400 °C with 60 mg of precalcined powder (800 °C for 4 h), in which the majority of organics had been removed. The heating rate was 10 °C/min in air using a NETZSCH model DSC 404 instrument (NETZSCH-Gerätebau GmbH, Wittelsbacherstraße Germany) with an alumina crucible. Sapphire (Al_2O_3) was used as a calibration standard. Thermogravimetric analysis (TGA) was also undertaken from room temperature up to 1500 °C using 60 mg of precalcined powder in air with a heating rate of 10 °C/min using a SETARAM TAG 24 (Caluire, France) with an alumina crucible.

Raman spectra were collected from powder samples at room temperature using the Renishaw inVia Raman spectrometer equipped with an argon ion laser (514 nm) and a Peltier cooled charge-coupled device (CCD) detector (Renishaw plc, Old Town, Gloucestershire, U.K.). Stokes shifted Raman spectra were collected in the static mode in the range of ~100–1000 cm^{-1} with a spectral resolution of 1.7 cm^{-1} for the 1800 l/mm grating. The spot size was around 1.5 μm for 50× magnification.

X-ray diffraction patterns were recorded using a BRUKER D8 instrument, with weighted Cu Kα radiation (λ = 1.5418 Å), between an angular range of 5–120° (2θ), with a step size of 0.02° and an acquisition time of 5 s per step. Refinements were carried out using the Rietveld method implemented in the program Rietica (version 1.7.7).[21] The peak shape was modeled using a pseudo-Voigt function with Howard asymmetry, with the background modeled using a fifth-order polynomial. All atomic displacement parameters (ADPs) were taken to be isotropic with the three oxygen ADPs constrained to be equal, and refined with the other profile and structural parameters.

Scanning electron microscopy (SEM) was used to analyze the microstructure and phase composition of the pelletized samples via energy dispersive spectra (EDS). Samples were mounted in an epoxy resin and polished to a 1 μm diamond finish. A thin carbon film (~5 nm) was deposited onto the polished surface for charge neutralization. The polished sections were examined in a Zeiss Ultra Plus scanning electron microscope (Carl Zeiss NTS GmbH, Oberkochen, Germany) operating at 15 kV equipped with an Oxford Instruments X-Max 80 mm^2 SDD X-ray microanalysis system. Semiquantitative analysis was performed using the Oxford Instruments INCA software. A copper metal standard was used for the Quant Optimization to ensure the best fit of the stored profiles within the software. The analytical errors due to spectrum processing are approximately 1% relative for both Ce and Ti. However, the actual systematic errors are much higher than this as standards were not employed in the particular procedures used here. Therefore, it was not possible to determine slight variations in the Ti/Ce ratio from the ideal value of 2.

X-ray absorption near-edge structure (XANES) analysis was carried out at beamline 16A1 at the National Synchrotron Radiation Research Center (NSRRC) in Hsinchu, Taiwan.[22] The Ce L_3-edge spectra were obtained from five samples sintered between 800 and 1350 °C plus four cerium 3+ and 4+ standards ($CeAlO_3$, CeO_2, $SrCeO_3$, and $La_2Ce_2O_7$), in fluorescence mode using a Lytle detector from powder samples dispersed on Kapton tape. Energy steps as small as 0.2 eV were employed near the absorption edge with a counting time of 2 s per step. The energy scale was calibrated using the K-edge of a pure Cr foil with the maximum in the first derivative set to 5989.2 eV. Background subtraction, normalization, and linear combination fitting were performed using the Athena software program.[23]

Sintered powders (1350 °C for 50 h) were pelletized using a uniaxial press at pressures between 2.0 and 2.5 MPa. Sample disks were annealed at 1350 °C for 50 h in air. Archimedes' displacement method, using distilled water, was used to determine the bulk density and apparent porosity of the sintered sample. Bulk density (D_b) refers to the ratio of the mass of a material to its bulk volume. Apparent porosity (P_a) refers to the percentage ratio of the volume of open pores in a material to the bulk volume of that material. Theoretical density was calculated from unit cell parameters obtained following Rietveld refinement of XRD data.

3. RESULTS AND DISCUSSION

Using traditional mixed-oxide processing, $CeTi_2O_6$ formation occurs via solid-state reaction only after extended sintering time (of more than 4 days) at high temperature[6,7,11] owing to the low specific surface area of the oxides at which diffusion reaction occurs. Following intermittent quenching/cooling, and grinding/ball milling in organic solvent (to preserve the stoichiometry of the components), repelleting is also required to prepare a bulk ceramic. In this study, however, the precursors of the two components were mixed in an aqueous medium, which ensures the complete interaction between

dx.doi.org/10.1021/ic500563j | Inorg. Chem. 2014, 53, 6761–6768

reactants. Even though the detailed reaction mechanism and the exact formula of the complex compound are unknown, it is reasonable to propose that negatively charged anions $[Tyzor\ LA]^{2-}$ and Ce^{3+} cations in aqueous solution potentially form complex compounds during the drying process. Thus, $[-Ti-O-Ce-O-Ti-]_n$ bonds are likely to be formed after high-temperature treatment. After heat treatment at 800 °C, almost all organic species are removed,[20] and brannerite-structured $CeTi_2O_6$ is formed as well as small amounts of discrete metal oxides (CeO_2 and/or TiO_2) based on XRD and SEM results, as summarized in Table 1 along with the results of density measurements.

Figure 1 shows the XRD patterns of the $CeTi_{2.0-2.2}$ oxide powders sintered at 1350 °C for 50 h. The samples were

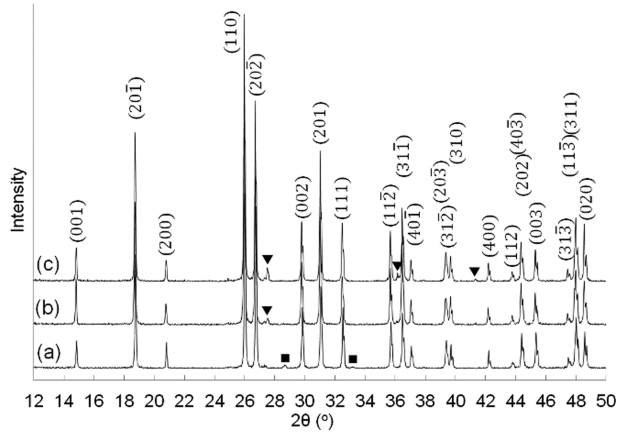

Figure 1. XRD patterns of powders sintered at 1350 °C for 50 h: (a) $CeTi_{2.0}$, (b) $CeTi_{2.1}$, (c) $CeTi_{2.2}$. (▼): rutile-type TiO_2; (■): CeO_2.

identified by laboratory XRD as near single phase materials with the brannerite structure. All patterns are refined using the Rietveld method based on the monoclinic structure in space group *C*2/*m*; a typical fit is shown in Figure 2 along with a

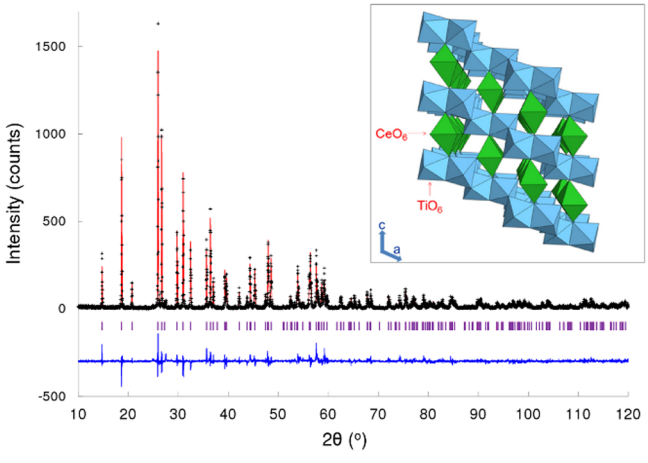

Figure 2. XRD pattern recorded at room temperature from $CeTi_{2.1}$ powder sintered at 1350 °C for 50 h. The black crosses represent the observed data, and the red solid line is the fit obtained by the Rietveld method using the monoclinic structure in *C*2/*m*. The purple vertical markers beneath the pattern show the peak positions expected in the structure, and the blue line records the difference between the observed and the calculated patterns. The inset shows the $CeTi_2O_6$ structure viewed along the *b* axis.

drawing of the $CeTi_2O_6$ crystal structure. In addition to the main phase, a trace amount of cerium dioxide (CeO_2, JCPDS card no. 00-001-0800, space group $Fd\bar{3}m$) was observed in the $CeTi_{2.0}$ oxide sample, while a trace amount of rutile (TiO_2, JCPDS card no. 01-089-4920, space group $P4_2/mnm$) was observed in the $CeTi_{2.1}$ and $CeTi_{2.2}$ oxide samples. The presence of CeO_2 impurity in the $CeTi_{2.0}$ sample seems to suggest that the brannerite main phase is slightly Ce-deficient as previously reported.[7] Therefore, we have refined the site occupancy of Ce (and constrained O1 site accordingly to maintain electroneutrality), using the same protocol as that by Stennett et al.;[7] the results confirm Ce deficiency in all our samples (see Table 2). However, due to limited X-ray scattering power for oxygen (especially in the presence of much heavier cations such as Ce), our results are not as accurate as those in ref 7, where neutron powder diffraction was utilized (the "real" error is expected to be much larger than the statistical error quoted in Table 2). Given that rutile impurity was observed in the $CeTi_{2.1}$ and $CeTi_{2.2}$ samples, the degree of non-stoichiometry is expected to be small, and hence, the stoichiometric molecular formula ($CeTi_2O_6$) is still used in the current paper to describe the brannerite samples. The brannerite unit cell dimensions were determined from the Rietveld refinement, and the results are in good agreement with previously published data (Table 2).

Figure 3 displays the XRD patterns of $CeTi_{2.1}$ oxide powder samples sintered for 12 h between 800 and 1400 °C. At all sintering temperatures except 1400 °C, the XRD patterns show peaks corresponding to the brannerite structure. This highlights the exceptional advantage of this synthetic procedure with brannerite forming at temperatures as low as 800 °C. Rutile-type TiO_2 and/or CeO_2 were observed as minor phases. Heat treatment at 1400 °C led to the constituent oxides (CeO_2 and TiO_2) being the main phases in the X-ray diffraction pattern (Figure 3, pattern f).

Thermal analysis was further used to investigate thermal behavior at high temperature. The DSC curve for the $CeTi_{2.1}$ oxide powder, following heat treatment at 800 °C for 4 h, is displayed in Figure 4a. The broad DSC endothermic feature between 800 and 1300 °C appears to correspond to the complete crystallization of brannerite structured $CeTi_2O_6$ at high temperature as well as the gradual elimination of carbon char,[20] which was introduced by the titanium precursor. The endothermic peak at approximately 1375 °C is attributed to sample melting and phase changing. In order to confirm melting, 1 g of the powder presintered at 1300 °C for 50 h was heat-treated in a platinum crucible at 1400 °C for 12 h. After cooling to room temperature, it was observed that the powder had melted to form a glassy looking solid ceramic. X-ray analysis of the resultant solid (Figure 3, pattern f) revealed only CeO_2, TiO_2, and minor brannerite ($CeTi_2O_6$). Therefore, the brannerite structure is expected to collapse into mainly binary oxides, leaving only minor amounts of brannerite at temperatures > 1375 °C. A similar observation was made in an early study[24] in which a mixture of CeO_2 and TiO_2 in a 1:2 molar ratio was heated to melting in air at 1400 °C and then cooled rapidly. The authors noted CeO_2 and TiO_2 in the X-ray patterns together with an unknown compound, which could be indexed as brannerite. It should also be mentioned here that, in this early work, no ternary chemical compounds were observed following heat treatment of the $1CeO_2 + 2TiO_2$ mixture between 1000 and 1300 °C under oxidizing conditions. As the melting point of TiO_2 and CeO_2 is 1843 and 2400 °C,

dx.doi.org/10.1021/ic500563j | Inorg. Chem. 2014, 53, 6761−6768

Table 2. Refined Unit Cell Parameters Determined from Rietveld Analysis of Laboratory XRD Data

	experimental data of this work			ref 7	ref 8	ref 11	ref 19
	$CeTi_{2.0}$	$CeTi_{2.1}$	$CeTi_{2.2}$	$Ce_{0.975}Ti_2O_{5.95}$	$CeTi_2O_6$	$CeTi_2O_6$	$CeTi_2O_6$
a (Å)	9.8338(2)	9.8316(2)	9.8313(2)	9.8320(1)	9.815(6)	9.8305(5)	9.817(1)
b (Å)	3.7544(1)	3.7538(1)	3.7540(1)	3.75287(6)	3.768(2)	3.7536(1)	3.7354(3)
c (Å)	6.8879(1)	6.8876(1)	6.8877(1)	6.8852(1)	6.925(5)	6.8919(2)	6.853(1)
β (deg)	119.217(1)	119.214(1)	119.213(1)	119.230(1)	118.92(2)	119.203(2)	119.0(1)
V (Å^3)	221.95(1)	221.86(1)	221.87(1)				
Ce occupancy	0.940(4)	0.956(4)	0.908(4)	0.976(3)			

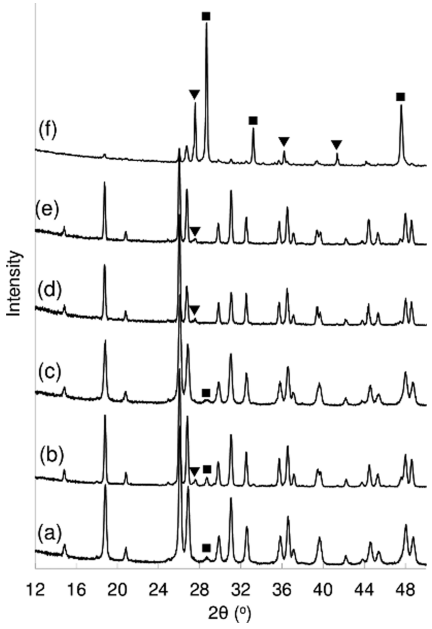

Figure 3. XRD patterns of $CeTi_{2.1}$ powders sintered for 12 h at (a) 800, (b) 1000, (c) 1200, (d) 1300, (e) 1350, and (f) 1400 °C. (▼): rutile-type TiO_2; (■): CeO_2.

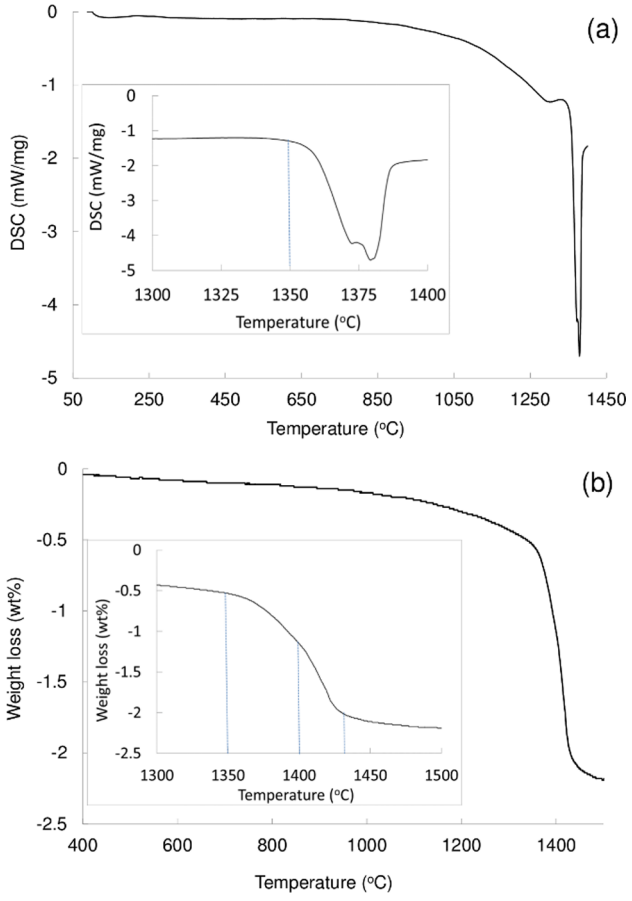

Figure 4. (a) DSC and (b) TGA of $CeTi_{2.1}$ powder that has been heat-treated at 800 °C for 4 h.

respectively,[25] it is likely that the "unknown" compound, consistent with $CeTi_2O_6$ brannerite, was formed between 1300 and 1400 °C before melting at ~1400 °C. TGA of the $CeTi_{2.1}$ oxide powder that had been heat-treated at 800 °C for 4 h was assessed up to 1500 °C in air (Figure 4b). The results show a gradual mass loss of ~0.4% between room temperature and 1300 °C due to the elimination of carbon char. A second mass loss of ~1.7% is apparent between 1300 and 1450 °C, where sample melting and phase changing occur. This mass loss is likely to be due to the partial loss of oxygen from the reduction of Ce^{4+} to Ce^{3+}, as reported in zirconia–ceria solid solution at elevated temperatures;[26,27] a complete reduction from Ce^{4+} to Ce^{3+} would result in a mass loss of 2.4% according to calculations.

While XRD is more sensitive to disorder in the cation sublattice than the anion sublattice, vibrational spectroscopy is very sensitive to the short-range environment of oxygen around the cations. Frequency bands in Raman and IR are sensitive to coordination geometry and oxidation states and thus are able to show the vibrational modes of various XO_6 octahedral units comprising the brannerite lattice.

The structure of $CeTi_2O_6$ is generally described as being composed of CeO_6 and TiO_6 polyhedra (see inset of Figure 2). Factor group analysis for this structure ($C2/m$ (C^3_{2h}) space group) forecasts a total of $3N$ (N denotes the number of atoms in the molecule) = $8A_g + 4B_g + 5A_u + 10B_u$ Brillouin zone center modes.[28] These modes can be subdivided into $A_u + 2B_u$ and $2A_g + B_g + A_u + 2B_u$ translations of the Ce^{4+} and Ti^{4+} cations, respectively. The remaining modes ($6A_g + 3B_g + 3A_u + 6B_u$) correspond to vibrations of the oxygen atoms. The A_g and B_g modes are Raman-active, whereas the A_u and B_u modes are IR-active. It is also noted that, among the translational modes, two modes ($A_u + 2B_u$) belong to the acoustic branches.[28]

Raman spectra of the three oxide powders ($CeTi_{2.0-2.2}$) sintered at 1350 °C for 50 h (Figure 5) are nearly identical. Out of 12 theoretically predicted Raman modes ($8A_g + 4B_g$), 9 active Raman modes were detected. Two weak Raman bands are assigned to the stretching vibrations of the Ti–O–Ti units: the 768 cm^{-1} band is due to an asymmetric stretching (B_g) mode and the 488 cm^{-1} band is due to the symmetric (A_g) vibration.[28−31] Two Raman A_g modes at 272 and 334 cm^{-1} and one B_g mode at 372 cm^{-1} are due to a combination of deformation vibrations of the Ti–O–Ti units (predominantly at higher frequencies) and stretching modes of CeO_6 octahedra

dx.doi.org/10.1021/ic500563j | Inorg. Chem. 2014, 53, 6761−6768

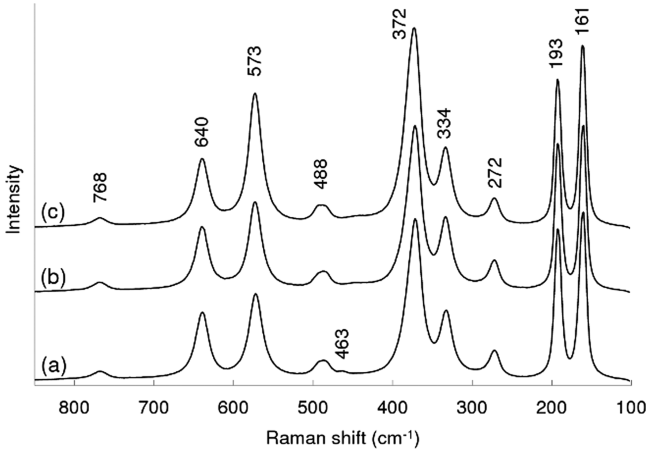

Figure 5. Raman spectra of powders sintered at 1350 °C for 50 h: (a) $CeTi_{2.0}$, (b) $CeTi_{2.1}$, (c) $CeTi_{2.2}$.

(predominantly at lower frequency).[29,30] The strong band at 573 cm^{-1} and the medium intensity band at 640 cm^{-1} (B_g mode) correspond to the stretching vibrations of the double Ti_2O_2 bridges (generated by the edge-sharing between pairs of octahedra).[30,31] Raman lines below 200 cm^{-1} are generally attributed to the external (lattice) modes.[28−31] In addition, a very weak peak observed around 463 cm^{-1} (Figure 5, spectrum a) belongs to pure cubic CeO_2. Interestingly, rutile TiO_2 as a minor phase was not detected by Raman spectroscopy for either $CeTi_{2.1}$ or $CeTi_{2.2}$ oxide sample (Figure 5, spectra b and c), in contrast to the XRD results (Figure 1, patterns b and c).

Raman spectra of the $CeTi_{2.1}$ oxide powder sintered at 800−1400 °C for 12 h (Figure 6) show several important features. Powders sintered at temperatures ≤ 1350 °C show very similar Raman patterns (Figure 6, spectra a−e) with the major peaks observed at 161, 193, 272, 334, 372, 488, 573, 640, and 768 cm^{-1}. For powders sintered at temperatures of 800 and 1200 °C, a small Raman peak located around 145 cm^{-1} was observed and consistent with a trace amount of anatase TiO_2 (which has a very strong peak around this wavenumber),[32] though XRD measurements did not detect the anatase phase possibly due to its low concentration within the sample. The Raman peak at 463 cm^{-1} (Figure 6, spectrum b) is assigned to pure cubic CeO_2 (space group $Fd\bar{3}m$),[33,34] which is in agreement with XRD results discussed above. The Raman spectrum for the powder heat-treated at 1400 °C (Figure 6, spectrum f) is significantly different from those sintered at temperatures ≤ 1350 °C. The 610 cm^{-1} peak and a shoulder around 440 cm^{-1} are due to the TiO_2 rutile phase.[32,34] A very broad peak centered at approximately 237 cm^{-1} is also representative of the rutile TiO_2 and due to a disorder-induced scattering.[34] A very strong peak at 463 cm^{-1} is assigned to pure cubic CeO_2. These findings are in an excellent agreement with the XRD data (Figure 3, pattern f), which clearly indicate the presence of CeO_2 and TiO_2 major phases as well as minor brannerite after heat treatment at 1400 °C. The simulated Raman spectrum using density functional theory (DFT) is discussed in the Supporting Information (Figure S1).

Far-IR spectra of the three oxide samples ($CeTi_{2.0-2.2}$) sintered at 1350 °C for 50 h and the $CeTi_{2.1}$ sample heat-treated at 1400 °C for 12 h were obtained, and results are presented in the Supporting Information (Figure S2). The far-IR profiles of these samples are similar to those of $ThTi_2O_6$ and $CeTi_2O_6$, as previously reported.[2,8]

SAED patterns were also obtained from three different Ce-brannerite powders sintered at 1350 °C for 50 h ($CeTi_{2.0}$, $CeTi_{2.1}$, and $CeTi_{2.2}$). The SAED results for the ⟨001⟩ and ⟨110⟩ zone axes are displayed in Figure S3 (Supporting Information) along with nondynamical calculated patterns. In general, all SAED patterns show sharp Bragg reflections consistent with the brannerite structure in all samples.

Figure 7 shows the Ce L_3-edge XANES spectra of five $CeTi_{2.1}$ samples sintered at 800−1350 °C for 12 h, along with

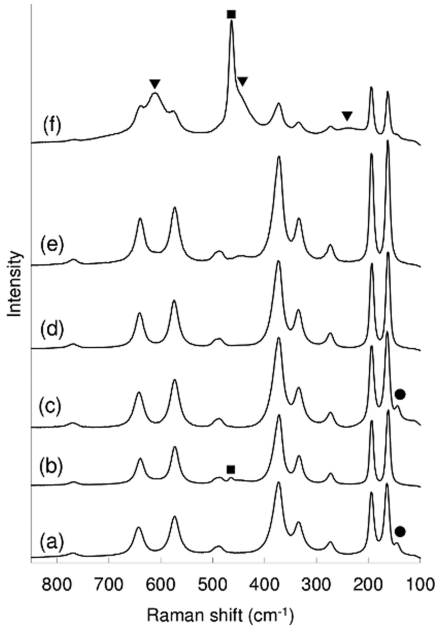

Figure 6. Raman spectra of $CeTi_{2.1}$ powders sintered for 12 h at (a) 800, (b) 1000, (c) 1200, (d) 1300, (e) 1350, and (f) 1400 °C. (▼): rutile-type TiO_2; (●): anatase-type TiO_2; (■): CeO_2.

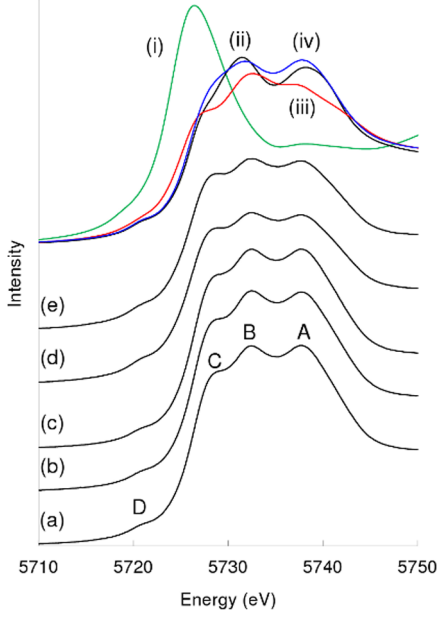

Figure 7. Ce L_3-edge XANES spectra of $CeTi_{2.1}$ powders sintered for 12 h at (a) 800, (b) 1000, (c) 1200, (d) 1300, and (e) 1350 °C, as well as Ce standard powders: (i) $CeAlO_3$ (green line), (ii) CeO_2 (black line), (iii) $SrCeO_3$ (red line), (iv) $La_2Ce_2O_7$ (blue line).

dx.doi.org/10.1021/ic500563j | Inorg. Chem. 2014, 53, 6761−6768

those of the Ce^{3+} ($CeAlO_3$) and Ce^{4+} (CeO_2, $SrCeO_3$, and $La_2Ce_2O_7$) standards. The Ce L_3-edge spectra result predominantly from dipole transitions of the Ce $2p_{3/2}$ electrons into the empty 5d states mixed in the conduction band, i.e., probing the unoccupied electronic states with d symmetries. The Ce^{3+} spectrum (such as that of $CeAlO_3$ and $Ce_{1/3}TaO_3$[35]) shows a single strong "white line" at the edge corresponding to the $2p^64f^15d^0 \rightarrow 2p^54f^15d^1$ transition.[7] In contrast, four peaks (labeled as A, B, C, and D) are observed at the L_3-edge of Ce^{4+}-containing samples, such as CeO_2, $La_2Ce_2O_7$, $SrCeO_3$, and $BaCeO_3$[36]). Peaks A and B are assigned to the transition from the initial $2p^64f^05d^0$ state to the final $2p^54f^05d^1$ and $2p^54f^1\underline{L}^15d^1$ states ($\underline{L}$ denotes a ligand hole), respectively.[7] Peak C is believed to originate from the $2p^54f^2\underline{L}^25d^1$ configuration, and peak D is associated with a quadrupole transition.[7] The noticeable difference in the line shape of the Ce L_3-edge spectra for the three Ce^{4+} standards measured in this work has been attributed to the difference in the Ce−O coordination number; peak C is more prominent and better resolved for Ce^{4+} in 6-fold coordination.[7] As shown in Figure 7, the Ce L_3-edge XANES spectra obtained from all five $CeTi_{2.1}$ samples sintered at different temperatures are essentially identical and closely resemble that of $SrCeO_3$, consistent with the presence of six-coordinated Ce^{4+} in these brannerite samples. It should be mentioned that a recent study has concluded that quenched $CeTi_2O_6$ samples are slightly O-deficient and charge-compensated by Ce^{3+}.[6] Although we cannot rule out the presence of Ce^{3+} completely due to the detection limit of XANES, our samples are unlikely to contain any Ce^{3+} considering that all samples were furnace-cooled in air, *not* quenched as in ref 6. This is supported by linear combination fits of the XANES spectra (a typical fit is shown in Figure S4, Supporting Information), which suggest the amount of Ce^{3+} component, if any, to be within the experimental uncertainty.

Powders with the brannerite structure (sintered at 1350 °C for 50 h) were pressed into pellets and further annealed at 1350 °C for 50 h in order to produce bulk brannerite monoliths. From the SEM micrographs, it is evident that all samples contain around 10−20% porosity (given by the dark areas in Figure 8). The image collected for each sample with the backscatter detector confirmed the presence of the main brannerite phase together with trace amounts of either CeO_2 or TiO_2. The SEM image of a fractured surface of the sintered $CeTi_{2.1}$ pellet is given in Figure 9, being a representative example of the fracture pattern of the sintered ceramics. There is a mix of transgranular and intergranular fracture, indicating good adhesion between the grains. The sample appears to have an average grain size of approximately 10−20 μm. Bulk density and apparent porosity were measured and are displayed in Table 1. The relative density is over 82% of the theroreical value. This relatively low bulk density is a result of the particle size and size distribution not being optimized, leaving larger voids in the pelletized powder when compacted.

Ce(III) generally forms thermodynamically very stable Ce(IV) dioxide when heated in the presence of an oxidizing atmosphere. CeO_2 once formed is quite unreactive even as a finely dispersed powder and does not tend to form polynary compounds. As a result, the formation of a stable brannerite $CeTi_2O_6$ via solid-state reaction between CeO_2 and TiO_2 requires high-temperature treatment (1300−1350 °C).[34,37] As the temperature of the system increases, the equilibrium shifts toward the reduced state.[6] Thus, heat treatment at temperatures above 1350 °C could introduce oxygen vacancies and the

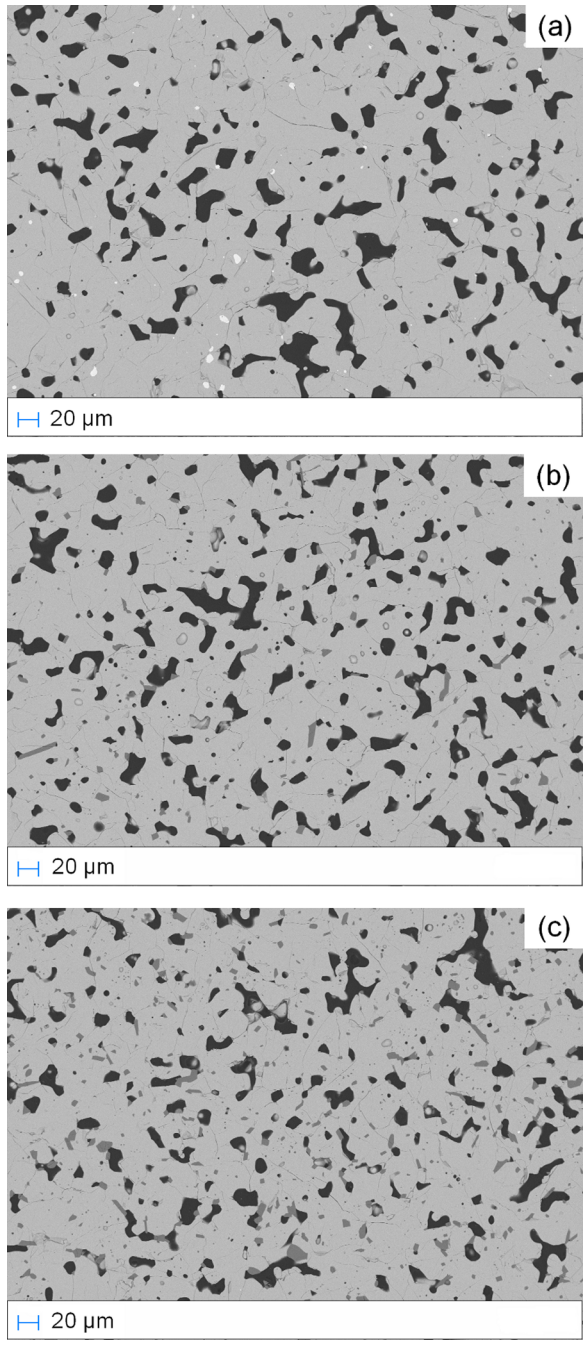

Figure 8. Backscattered scanning electron micrographs of the polished surfaces of pellet samples annealed at 1350 °C for 50 h after sintering powders at 1350 °C for 50 h: (a) $CeTi_{2.0}$, (b) $CeTi_{2.1}$, and (c) $CeTi_{2.2}$. The main phase is $CeTi_2O_6$, dark-gray regions are rutile-type TiO_2, the white phase is CeO_2, and black areas are pores.

Ce^{3+} ions, leading to a distortion of the local symmetry.[6] This can cause a change in the Ce−O bond length (lattice distortion) and the overall lattice parameter, because Ce^{3+} ions have a higher ionic radius (1.01 Å) as compared to the Ce^{4+} ions (0.87 Å) with a six-coordination environment according to Shannon.[38] We have not confirmed the presence of Ce^{3+} ions at high sintering temperatures because the Ce^{3+} might have reoxidized to Ce^{4+} during the cooling period. Therefore, detailed structural studies with in situ investigation at high temperatures are required to probe the structural

dx.doi.org/10.1021/ic500563j | Inorg. Chem. 2014, 53, 6761−6768

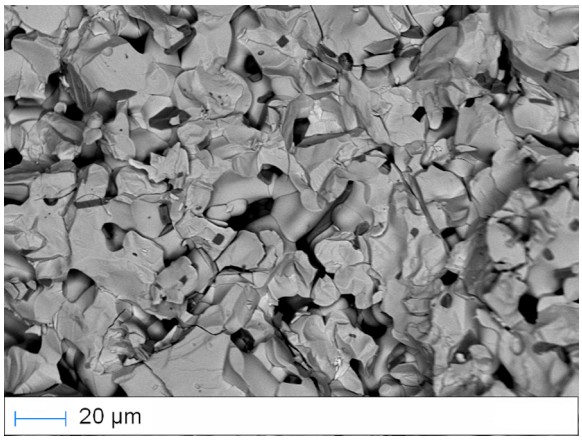

Figure 9. Backscattered scanning electron micrograph showing the fractured surface of $CeTi_{2.1}$ pellet sample annealed at 1350 °C for 50 h after sintering powder at 1350 °C for 50 h.

evolution and composition variation with temperature and dwell time.

4. CONCLUSIONS

Cerium titanate $CeTi_2O_6$ was synthesized in an aqueous media using non-moisture-sensitive titanium precursor (Tyzor LA) and cerium(III) nitrate hexahydrate. The chemical reaction took place at the molecular level, which ensured homogeneity of the synthesized powder. The brannerite crystalline structure was formed upon calcination in air at temperatures as low as 800 °C. XRD, Raman, and SAED techniques confirmed the formation of the brannerite structure. XANES results indicated that the Ce valence was predominantly 4+. $CeTi_2O_6$ powder compacted and annealed at 1350 °C for 50 h yielded relative densities of >80%. In addition, Rietveld refinements suggested the possibility of slight Ce deficiency in the brannerite phase. Further studies are planned to improve the relative density through optimized particle size, size distribution, and sintering protocols, such as hot isostatic pressing, and to dope brannerite with actinides.

■ ASSOCIATED CONTENT

Supporting Information

Raman simulation, far-infrared, selected area electron diffraction, and linear combination fits of XANES spectra. This material is available free of charge via the Internet at http://pubs.acs.org.

■ AUTHOR INFORMATION

Corresponding Author

*E-mail: lnk@ansto.gov.au. Tel.: +61 2 9717 3630. Fax: +61 2 9717 9225.

Notes

The authors declare no competing financial interest.

■ ACKNOWLEDGMENTS

We thank Dr. Eric R. Vance for helpful discussions. XANES data were obtained with the assistance of Drs. Peter Blanchard, Ling-Yung Jang, and Samuel Liu. XANES work carried out in Taiwan was supported by the International Synchrotron Access Program (ISAP), funded by the Australian Synchrotron.

■ REFERENCES

(1) Kidchob, T.; Malfatti, L.; Marongiu, D.; Enzo, S.; Innocenzi, P. *Thin Solid Films* **2010**, *518*, 1653−1657.
(2) Kidchob, T.; Malfatti, L.; Marongiu, D.; Enzo, S.; Innocenzi, P. *J. Sol-Gel Sci. Technol.* **2009**, *52*, 356−361.
(3) Verma, A.; Goyal, A.; Sharma, R. K. *Thin Solid Films* **2008**, *516*, 4925−4933.
(4) Verma, A.; Srivastava, A. K.; Sood, K. N. *Solid State Ionics* **2007**, *178*, 1288−1296.
(5) Lumpkin, G. R.; Leung, S. H. F.; Ferenczy, J. *Chem. Geol.* **2012**, *291*, 55−68.
(6) Huynh, L. T.; Eger, S. B.; Walker, J. D. S.; Hayes, J. R.; Gaultois, M. W.; Grosvenor, A. P. *Solid State Sci.* **2012**, *14*, 761−767.
(7) Stennett, M. C.; Freeman, C. L.; Gandy, A. S.; Hyatt, N. C. *J. Solid State Chem.* **2012**, *192*, 172−178.
(8) Zhang, F. X.; Lang, M.; Liu, Z.; Ewing, R. C. *J. Solid State Chem.* **2011**, *184*, 2834−2839.
(9) Donaldson, M. H.; Stevens, R.; Lang, B. E.; Boerio-Goates, J.; Woodfield, B. F.; Putnam, R. L.; Navrotsky, A. *J. Therm. Anal. Calorim.* **2005**, *81*, 617−625.
(10) Otsuka-Yao-Matsuo, S.; Omata, T.; Yoshimura, M. *J. Alloys Compd.* **2004**, *376*, 262−267.
(11) Helean, K. B.; Navrotsky, A.; Lumpkin, G. R.; Colella, M.; Lian, J.; Ewing, R. C.; Ebbinghaus, B.; Catalano, J. G. *J. Nucl. Mater.* **2003**, *320*, 231−244.
(12) Lian, J.; Wang, L. M.; Lumpkin, G. R.; Ewing, R. C. *Nucl. Instrum. Methods Phys. Res., Sect. B* **2002**, *191*, 565−570.
(13) Lumpkin, G. R.; Smith, K. L.; Blackford, M. G. *J. Nucl. Mater.* **2001**, *289*, 177−187.
(14) Szymanski, J. T.; Scott, J. D. *Can. Miner.* **1982**, *20*, 271−279.
(15) James, M.; Carter, M. L.; Watson, J. N. *J. Solid State Chem.* **2003**, *174*, 329−333.
(16) Finnie, K. S.; Zhang, Z.; Vance, E. R.; Carter, M. L. *J. Nucl. Mater.* **2003**, *317*, 46−53.
(17) James, M.; Watson, J. N. *J. Solid State Chem.* **2002**, *165*, 261−265.
(18) Vance, E. R.; Watson, J. N.; Carter, M. L.; Day, R. A.; Begg, B. D. *J. Am. Ceram. Soc.* **2001**, *84*, 141−144.
(19) Yoshida, M.; Koyama, N.; Ashizawa, T.; Sakata, Y.; Imamura, H. *Jpn. J. Appl. Phys.* **2007**, *46*, 977−979.
(20) Kong, L.; Karatchevtseva, I.; Gregg, D. J.; Blackford, M. G.; Holmes, R.; Triani, G. *J. Am. Ceram. Soc.* **2013**, *96*, 935−941.
(21) Hunter, B. A.; Howard, C. J. *LHPM: A Computer Program for Rietveld Analysis of X-ray and Neutron Powder Diffraction Patterns*; Lucas Heights Research Laboratories: Sydney, Australia, 2000.
(22) Dann, T.-E.; Chung, S.-C.; Huang, L.-J.; Juang, J.-M.; Chen, C.-I.; Tsang, K.-L. *J. Synchrotron Radiat.* **1998**, *5*, 664−666.
(23) Ravel, B.; Newville, M. *J. Synchrotron Radiat.* **2005**, *12*, 537−541.
(24) Leonov, A. I.; Piryutko, M. M.; Keler, É. K. *Izv. Akad. Nauk. SSSR, Ser. Khim.* **1966**, *5*, 787−792.
(25) Lide, D. R., Ed. *CRC Handbook of Chemistry and Physics*, 88th ed.; CRC Press: Boca Raton, FL, 2008.
(26) Theunissen, G. S. A. M.; Winnubst, A. J. A.; Burggraaf, A. J. *J. Eur. Ceram. Soc.* **1992**, *9*, 251−263.
(27) Tadokoro, S. K.; Muccillo, E. N. S. *J. Eur. Ceram. Soc.* **2002**, *22*, 1723−1728.
(28) Knyazev, A. V.; Mączka, M.; Smirnova, N. N.; Macalik, L.; Kuznetsova, N. Y.; Letyanina, I. A. *J. Solid State Chem.* **2009**, *182*, 3003−3012.
(29) Amdouni, N.; Zarrouk, H.; Soulette, F.; Julien, C. M. *J. Mater. Chem.* **2003**, *13*, 2374−2380.
(30) Baran, E. J.; Cabello, C. I.; Nord, A. G. *J. Raman Spectrosc.* **1987**, *18*, 405−407.
(31) Zhang, Y.; Karatchevtseva, I.; Qin, M.; Middleburgh, S. C.; Lumpkin, G. R. *J. Nucl. Mater.* **2013**, *437*, 149−153.
(32) Orendorz, A.; Brodyanski, A.; Lösch, J.; Bai, L. H.; Chen, Z. H.; Le, Y. K.; Ziegler, C.; Gnaser, H. *Surf. Sci.* **2007**, *601*, 4390−4394.

(33) Fu, M.; Wei, L.; Li, Y.; Zhou, X.; Hao, S.; Li, Y. *Solid State Sci.* **2009**, *11*, 2133−2137.
(34) Martos, M.; Julián-López, B.; Folgado, J. V.; Cordoncillo, E.; Escribano, P. *Eur. J. Inorg. Chem.* **2008**, 3163−3171.
(35) Zhang, Z.; Kennedy, B. J.; Howard, C. J.; Jang, L. Y.; Knight, K. S.; Matsuda, M.; Miyake, M. *J. Phys.: Condens. Matter* **2010**, *22*, 445401.
(36) Zhou, Q.; Blanchard, P.; Kennedy, B. J.; Reynolds, E.; Zhang, Z.; Miiller, W.; Aitken, J. B.; Avdeev, M.; Jang, L.-Y.; Kimpton, J. A. *Chem. Mater.* **2012**, *24*, 2978−2986.
(37) Preuss, A.; Gruehn, R. *J. Solid State Chem.* **1994**, *110*, 363−369.
(38) Shannon, R. D. *Acta Crystallogr.* **1976**, *A32*, 751−767.